Deformation and Scattering in Graphene over Substrate Steps

T. Low, V. Perebeinos, J. Tersoff, and Ph. Avouris
IBM T. J. Watson Research Center, Yorktown Heights, New York 10598, USA
(Received 24 October 2011; published 1 March 2012)

The electrical properties of graphene depend sensitively on the substrate. For example, recent measurements of epitaxial graphene on SiC show resistance arising from steps on the substrate. Here we calculate the deformation of graphene at substrate steps, and the resulting electrical resistance, over a wide range of step heights. The elastic deformations contribute only a very small resistance at the step. However, for graphene on SiC(0001) there is strong substrate-induced doping, and this is substantially reduced on the lower side of the step where graphene pulls away from the substrate. The resulting resistance explains the experimental measurements.

DOI: 10.1103/PhysRevLett.108.096601 PACS numbers: 72.80.Vp, 61.48.Gh, 73.22.Pr, 81.05.ue

The advance of very high speed graphene electronics [1,2] depends on understanding and controlling the interaction of graphene with the supporting substrate. Electron mobility can vary over many orders of magnitude depending on the substrate [3–5]. Among other factors, morphological deformations of the graphene may limit mobility [6–10]. It is therefore important to determine how the substrate morphology affects transport in supported graphene.

Epitaxial graphene on SiC provides an ideal system in which to study the role of substrate morphology. SiC is a promising substrate because, in contrast to other approaches, it allows growth of epitaxial graphene directly on an insulating substrate [11]. However, epitaxial graphene on SiC substrates generally exhibits smaller carrier mobilities than exfoliated graphene on SiO_2 substrates [5,11–13]. The reason for this difference is not fully understood, but SiC substrates exhibit a high density of multilayer steps, which are implicated in the lower mobility. Several experiments show that resistance increases with step density [6], step heights [9], and step bunching [7,8]; and the local electrical resistance associated with individual substrate steps has recently been measured [9], by scanning potentiometry in a scanning tunneling microscope.

Here we study graphene over an abrupt substrate step, as illustrated in Fig. 1, calculating both the structural deformation and the resulting electrical resistance. The results are directly applicable to epitaxial graphene on SiC, and also show more generally how the morphology affects electrical transport. We find that very little resistance arises directly from the structural deformations, despite the strong curvature of graphene as it passes over a step. For SiC, we nevertheless find a substantial resistance associated with the step, in good agreement with experiment [9]. This resistance arises almost entirely from the electrical coupling between the graphene and substrate, which varies sharply in the vicinity of the step. Thus morphology plays a qualitatively different and far more important role in substrates such as SiC that dope the graphene or otherwise couple strongly, than it does for substrates such as SiO_2 that are electrically passive.

We begin by determining the graphene geometry as it passes over a substrate step. The graphene deformation is determined by a balance between the van der Waals (vdw) interaction, which favors conforming to the substrate, and elasticity, which favors keeping the graphene flat and smooth. Since the displacement field can vary on the atomic scale, we use an atomistic valence force model (VFM) to describe the elastic deformations [14]. The van der Waals interaction between graphene and substrate is modeled with the Lennard-Jones (LJ) 6–12 potential [15]. The parameters for our LJ model are determined by setting the equilibrium distance between graphene and substrate to $h_{\rm eq} \approx 3.4$Å [16], and the binding energy to $E_B \approx 40$ meV per atom [15,17]. The total energy is then simply the sum of these two contributions, $\mathcal{E} = \mathcal{E}_{\rm elas} + \mathcal{E}_{\rm vdw}$.

We calculate the minimum-energy geometry for graphene over a wide range of step height h_s, allowing the graphene to slide to relax any in-plane strain. The relaxed

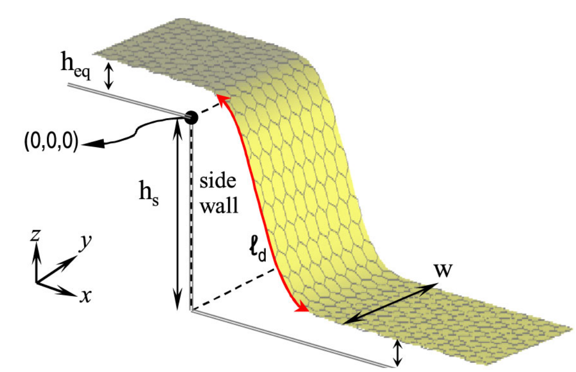

FIG. 1 (color online). Illustration of graphene over a substrate step. Here h_s is the step height and $h_{\rm eq}$ is the equilibrium distance of graphene from the substrate surface due to van der Waals interaction. ℓ_d is the length of graphene detachment from the substrate.

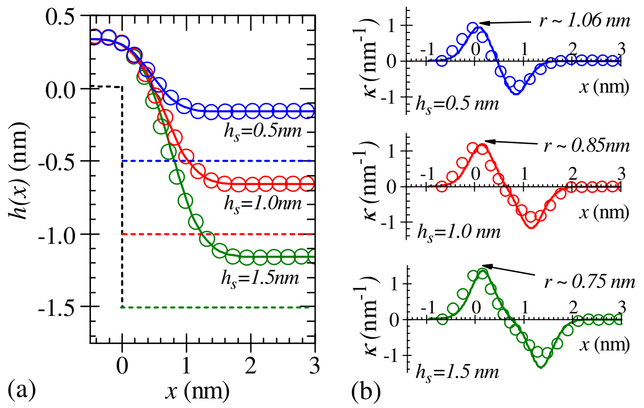

FIG. 2 (color online). (a) Graphene geometry $h(x)$ for various step heights as indicated. Symbols are the full numerical calculation. Solid lines are best fit using Eq. (1). The respective step profile are illustrated by dashed lines. (b) Corresponding curvature κ for geometries shown in (a), with lines and symbols as in (a). The minimum radius of curvature (inverse of maximum κ) is indicated.

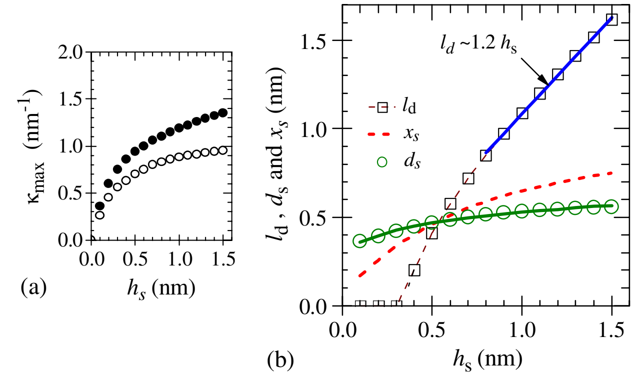

FIG. 3 (color online). (a) Numerically calculated maximum curvature κ_{max} for the upper edge (solid circles) and lower edge (open circles) of the step as function of step height h_s. Note that the often used approximation for curvature, $\kappa \approx \partial_x^2 h$, is only reasonable for h_s of few angstrom. Over the range of h_s of our interests, it grossly overestimates the real curvature due to the large gradients in our graphene geometries. (b) Dependence of graphene deformation on step height h_s. Graphene step width d_s and lateral shift x_s are obtained by fitting Eq. (1) to the relaxed geometry $h(x)$ obtained numerically. We also show the detachment length ℓ_d, i.e., the length of graphene separated from the substrate by $2h_{\text{eq}}$. Note that $\ell_d \approx 1.2h_s$ for large h_s. The step width d_s depends only weakly on step height.

geometries $h(x)$ for three step heights typical of SiC are plotted in Fig. 2(a). The presence of the atomic step increases the graphene area compared to when the substrate is flat. The extra length increases with h_s and was found to be 0.1, 0.3, and 0.6 nm, respectively. The nonlinear dependence reflects the increasing distortion (steeper slope) with increasing step height. The maximum slope is of order 1, confirming the need for a fully numerical treatment.

We find that the calculated geometries can be well approximated by a simple error function,

$$h(x) \approx -\frac{h_s}{2}\left[\operatorname{erf}\left(\frac{x - x_s}{d_s}\right) + 1\right] + h_{\text{eq}}. \qquad (1)$$

As shown in Fig. 2(b), even the variation in curvature across the step is well described by this simple functional form. The only noticeable discrepancy is that the error function is symmetric, while in the full calculation there is a slight asymmetry, with the maximum curvature induced at the upper edge of the step. For step height $h_s =$ 1.5 nm, we find a maximum curvature equivalent to that of a carbon nanotube of diameter 1.5 nm.

The maximum curvature κ_{max} as a function of step height h_s is plotted in Fig. 3(a), for both the lower and upper edge of the step. It is proportional to h_s in the small h_s limit. For the lower edge, the limit of large h_s corresponds to the well-known problem of peeling [18]. In this limit, κ_{max} approaches $\sqrt{2E_B/a\beta} \approx 1.2\ \text{nm}^{-1}$, where a is area per carbon atom and $\beta \approx 2.1$ eV [14] is the bending rigidity.

Figure 3(b) summarizes the dependence of the graphene deformation $h(x)$ on step height h_s, in terms of the parameters of Eq. (1). For a given step height, the characteristic step width d_s determines the maximum radius of curvature $r = 1/\kappa_{\text{max}}$. Another relevant length scale is the length ℓ_d over which the graphene is detached from the substrate. For concreteness we define ℓ_d to be the length of graphene separated by $2h_{\text{eq}}$ or more from the substrate surface. Figure 3(b) shows that ℓ_d remains zero at small h_s but begins to increase rapidly for $h_s > h_{\text{eq}}$. At larger step height we find that $\ell_d \sim 1.2h_s$, which proves important in later discussions.

Geometry-induced scattering.—Curvature results in band structure changes that can scatter electrons near the step. To examine this effect, after performing the geometry relaxation, we construct the Hamiltonian $\mathcal{H}$ within a nearest-neighbor Slater-Koster parameterized sp^3 tight-binding model [19]. We then calculate the transmission and the electrical resistance $\mathcal{R}$ using the nonequilibrium Green's function formalism [20,21] in the limit of small voltage across the step and no inelastic scattering at the step. We use the known Fermi level [16,22] of $E_f =$ 0.45 eV for graphene on SiC (0001).

Since the maximum curvature increases with step height h_s, the resistance also increases. For a step height of 1.5 nm, we obtain a resistance $\sim$0.01 Ω-μm. Figure 4(a) includes results of a recent experiment [9], which employed scanning potentiometry in a scanning tunneling microscope to resolve the resistance in graphene due to individual substrate steps. The measured resistance $\mathcal{R}_{\text{exp}}$ has roughly linear dependence with step height h_s, $\sim$10 Ω-μm for each nanometer step height. Evidently, the resistance due to curvature alone cannot account for this large $\mathcal{R}_{\text{exp}}$. While π-σ hybridization can result in new scattering states in the vicinity of Dirac point [23], this

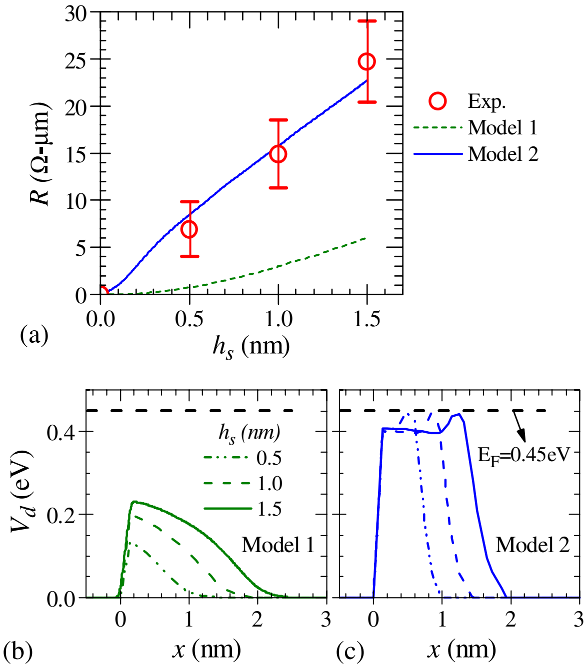

FIG. 4 (color online). (a) Resistance through graphene due to substrate step, $\mathcal{R}$, as function of step height h_s. Two electrostatic models for the doping variations are plotted, as described by Eq. (2) (model 1) and Eq. (3) (model 2). Experimental data [9] are plotted as circles, with statistical error bar indicated. (b) Potential profile $V_d(x)$ derived from Eq. (2) (model 1) for $h_0 = 0.5$, 1.0, and 1.5 nm. Dashed horizontal line indicates the Fermi level position. (c) Same as (b), but derived from Eq. (3) (model 2). The small hump observed for $V_d(x)$ near the top is an artifact of the polynomial form of $\Delta_c(h)$.

effect is significant only when $r \lesssim 5$Å [23]. Even for a very high step of $h_s = 1.5$ nm, we find that the minimum radius of curvature only shrinks to $r \approx 5$Å if we assume a much stronger van der Waals attraction, with a binding energy 80 meV, which seems unphysical.

In our calculations thus far, we have ignored possible in-plane strain inhomogeneities, which are known to result in electron scattering [24,25]. Because of the different thermal expansion coefficient between graphene and SiC, graphene can acquires a residual biaxial strain upon cooling if sliding is suppressed. Then due to the nonplanar geometry, graphene at the step could experience a uniaxial stress relative to the rest of the sheet. Graphene on SiC substrates is reported to have strains from 0.1%–1% as measured by Raman spectroscopy [26]. To estimate a very conservative upper bound for $\mathcal{R}$ due to strain inhomogeneity, we consider a local tensile strain of 1% along the detached region, with the step along the zigzag direction where the scattering effect is largest [24]. The result is $\mathcal{R} < 1$ Ω-μm. Thus some source of scattering much stronger than the geometrical deformations must be present to account for the measured resistance.

Electrostatic doping effects.—It is well known that when contacting graphene with metals, a difference in work function results in electrostatic doping [27–29]. In the case of SiC(0001), a similar doping occurs from the carbon buffer layer, which has a high density of weakly dispersive interface states [16,30]. This can be described by a capacitor model including quantum capacitance [31],

$$n(x) = \gamma\left(W_{sg} - \frac{e^2}{\epsilon_0} h(x)n(x) - \hbar v_f \sqrt{\pi n(x)}\right), \qquad (2)$$

where $n(x)$ is the electron density in graphene, W_{sg} is the work function difference between the carbon buffer layer and graphene, h is the distance between them, and γ is the buffer-layer density of states. We denote this as "model 1". In view of the flat bands [16,30], we take the limit of large γ and we adjust W_{sg} to reproduced the known doping at $h = h_{\text{eq}}$, corresponding to heavy n doping [16,22], with a Fermi level $E_f = 0.45$ eV. The vertical displacement $h(x)$ changes the capacitive coupling, leading to doping variations. Substituting the relaxed geometry $h(x)$ into Eq. (2), we calculate these variations. The associated potential shifts $V_d(x)$ are shown in Fig. 4(b) for different step heights. Increasing step height leads to larger detachment and doping variations. This translates to an increased $\mathcal{R}$ as shown in Fig. 4(a), still somewhat smaller than reported experimentally, but far larger than the scattering mechanisms previously discussed.

In studies of metal induced doping of graphene, Khomyakov and co-workers [28,29] reported that Eq. (2) could not properly describe the *ab initio* calculations of graphene on metals, presumably due to quantum mechanical effects such as wave function overlap and correlations. They suggested that the accuracy of Eq. (2) can be improved by the modification [28,29]

$$\begin{aligned} h(x) &\rightarrow h(x) + h^*, \\ W_{sg} &\rightarrow W_{sg} + \Delta_c(h) \end{aligned} \qquad (3)$$

with h^* and $\Delta_c(h)$ approximated as independent of the metal species. Since the corresponding values for SiC are not known, and the buffer layer has a large density of states the Fermi level, we simply use the values reported for metals in Refs. [28,29].

This "model 2" gives a stronger doping variation than the classical electrostatic model, as show in Fig. 4(c). The corresponding resistance is also increased for model 2, as shown in Fig. 4(a), giving excellent agreement with experiment. Indeed, we consider the degree of quantitative agreement between "model 2" and the experimental data to be somewhat fortuitous. Nevertheless, it is striking that, using the best approximations available, the modulation of local doping by the step can account for the observed resistance, while other mechanisms are all far too small.

In principle there could be additional electronic states associated with the step that would change the resistance, but it is not necessary to assume such states in order to explain the resistance. Here we assumed the vertical surface of the atomic step to be electrically inert. This is reasonable since the SiC $(000\bar{1})$ surface is electrically inert, and the extra states are associated with the buffer layer. In addition, our results are relatively robust against the uncertainties in the bending stiffness and the van der Waals binding energy. For example, if we assume an unreasonably large $E_B = 80$ meV instead of $E_B = 40$ meV, the detachment length for the largest step height decreases from 1.56 to 1.41 nm, suggesting a decrease in resistance of only $\approx 10\%$. A factor of 2 change in the assumed bending stiffness would have a similar effect.

As seen in Fig. 4(c), the graphene is almost fully depleted of carriers in the detached region. This suggests a simple model where the graphene is completely undoped over the detachment length ℓ_d. Our situation then resembles the problem of minimum conductivity, often discussed in the literature [32]. Transport in this regime is mediated by evanescent modes, but instead of an exponential decay the graphene bandstructure leads to a unique linear (''pseudodiffusive'') behavior [32], where $\mathcal{R} \approx \frac{\pi^2 \hbar}{2e^2} \ell_d$. This represents the upper bound for resistance due to doping variations, where the doping goes to zero in the detached region, and overestimates the calculations of ''model 2'' by about 50%. Combining this with our previous result that $\ell_d \approx 1.2 h_s$ explains the linear scaling of resistance with step height (i.e. $\mathcal{R}_{\mathrm{step}} \propto h_s$) observed in experiment.

Conclusions.—We examined the structural deformation of graphene crossing over a substrate step, and the various intrinsic mechanisms that may cause electron scattering at the step. We found that deformation gives only a small electron scattering. For graphene on SiC, where the substrate induces considerable doping, the dominant mechanism is rather the abrupt variation in potential and doping due to detachment of the graphene from the substrate as it passes over a step. Our results are consistent with the various experimental observations, i.e., that $\mathcal{R}_{\mathrm{step}}$ increases with step density [6], step heights [9], step bunching [7,8], all of which are characterized by increasing ℓ_d.

We thank the authors of Ref. [9] for providing experimental data prior to publication. T. L acknowledges use of a computing cluster provided by Network for Computational Nanotechnology, and partial funding from INDEX-NRI.

[1] P. Avouris, Nano Lett. **10**, 4285 (2010).
[2] Y. M. Lin *et al.*, Science **332**, 1294 (2011).
[3] A. H. C. Neto, F. Guinea, N. M. Peres, K. S. Novoselov, and A. K. Geim, Rev. Mod. Phys. **81**, 109 (2009).
[4] C. R. Dean *et al.*, Nature Nanotech. **5**, 722 (2010).
[5] C. Berger, Z. Song, X. Li, X. Wu, N. Brown, C. Naud, D. Mayou, T. Li, J. Hass, and A. Marchenkov *et al.*, Science **312**, 1191 (2006).
[6] C. Dimitrakopoulos, A. Grill, T. McArdle, Z. Liu, R. Wisnieff, and D. A. Antoniadis, Appl. Phys. Lett. **98**, 222105 (2011).
[7] Y. M. Lin, D. B. Farmer, K. A. Jenkins, Y. Wu, J. L. Tedesco, R. L. Myers-Ward, C. R. Eddy, D. K. Gaskill, C. Dimitrakopoulos, and P. Avouris, IEEE Electron Device Lett. (to be published).
[8] S. E. Bryan, Y. Yang, and R. Murali, J. Phys. Chem. C **115**, 10 230 (2011).
[9] S. Ji, J. B. Hannon, R. M. Tromp, V. Perebeinos, J. Tersoff, and F. M. Ross, Nature Mater. **11**, 114 (2011).
[10] K. Kim, Z. Lee, B. D. Malone, K. T. Chan, B. Aleman, W. Regan, W. Gannett, M. F. Crommie, M. L. Cohen, and A. Zettl, Phys. Rev. B **83**, 245433 (2011).
[11] K. V. Emtsev *et al.*, Nature Mater. **8**, 203 (2009).
[12] J. L. Tedesco, B. L. VanMil, R. L. Myers-Ward, J. M. McCrate, S. A. Kitt, P. M. Campbell, G. G. Jernigan, J. C. Culbertson, C. R. Eddy, and D. K. Gaskill, Appl. Phys. Lett. **95**, 122102 (2009).
[13] J. A. Robinson *et al.*, Nano Lett. **9**, 2873 (2009).
[14] V. Perebeinos and J. Tersoff, Phys. Rev. B **79**, 241409(R) (2009).
[15] L. A. Girifalco and R. A. Lad, J. Chem. Phys. **25**, 693 (1956).
[16] A. Mattausch and O. Pankratov, Phys. Rev. Lett. **99**, 076802 (2007).
[17] R. Zacharia, H. Ulbricht, and T. Hertel, Phys. Rev. B **69**, 155406 (2004).
[18] L. D. Landau and E. M. Lifshitz, *Course of Theoretical Phys.* 7, 45 (Butterworth-Heinemann, Cambridge, UK, 1986).
[19] D. Tomanek and S. G. Louie, Phys. Rev. B **37**, 8327 (1988).
[20] S. Datta, *Electronic Transport in Mesoscopic System* (Cambridge University Press, Cambridge, England, 1997).
[21] M. Di Ventra, *Electrical Transport in Nanoscale System* (Cambridge University Press, Cambridge, England, 2008).
[22] A. Bostwick, T. Ohta, T. Seyller, K. Horn, and E. Rotenberg, Nature Phys. **3**, 36 (2006).
[23] X. Blase, L. X. Benedict, E. L. Shirley, and S. G. Louie, Phys. Rev. Lett. **72**, 1878 (1994).
[24] M. M. Fogler, F. Guinea, and M. I. Katsnelson, Phys. Rev. Lett. **101**, 226804 (2008).
[25] V. M. Pereira and A. H. C. Neto, Phys. Rev. Lett. **103**, 046801 (2009).
[26] J. A. Robinson, C. P. Puls, N. E. Staley, J. P. Stitt, M. A. Fanton, K. V. Emtsev, T. Seyller, and Y. Liu, Nano Lett. **9**, 964 (2009).
[27] B. Huard, N. Stander, J. A. Sulpizio, and D. Goldhaber-Gordon, Phys. Rev. B **78**, 121402(R) (2008).
[28] P. A. Khomyakov, G. Giovannetti, P. C. Rusu, G. Brooks, J. van den Brink, and P. J. Kelly, Phys. Rev. B **79**, 195425 (2009).
[29] G. Giovannetti, P. A. Khomyakov, G. Brooks, V. M. Karpan, J. van den Brink, and P. J. Kelly, Phys. Rev. Lett. **101**, 026803 (2008).
[30] F. Varchon, R. Feng, J. Hass, X. Li, N. Nguyen, C. Naud, P. Mallet, J. Y. Veuillen, C. Berger, and E. H. Conrad *et al.*, Phys. Rev. Lett. **99**, 126805 (2007).
[31] S. Kopylov, A. Tzalenchuk, S. Kubatkin, and V. Fal'ko, Appl. Phys. Lett. **97**, 112109 (2010).
[32] J. Tworzydlo, B. Trauzettel, M. Titov, A. Rycerz, and C. W. J. Beenakker, Phys. Rev. Lett. **96**, 246802 (2006).